Article

ZnO/Ag Nanocomposites with Enhanced Antimicrobial Activity

Jaime Gonzalez Cuadra [1,*], Loredana Scalschi [2], Begonya Vicedo [2], Maxim Guc [3], Víctor Izquierdo-Roca [3], Samuel Porcar [1], Diego Fraga [1] and Juan B. Carda [1]

[1] Department of Inorganic and Organic Chemistry, Universitat Jaume I, Avenida Vicent Sos Baynat, s/n, 12071 Castellón de la Plana, Spain; saporcar@uji.es (S.P.); fraga@uji.es (D.F.); carda@uji.es (J.B.C.)

[2] Department of Biology, Biochemistry and Natural Sciences, Universitat Jaume I, Avenida Vicent Sos Baynat, s/n, 12071 Castellón de la Plana, Spain; scalschi@uji.es (L.S.); bvicedo@uji.es (B.V.)

[3] Catalonia Institute for Energy Research (IREC), Jardins de les Dones de Negre 1, 2ª pl., 08930 Sant Adrià de Besòs, Spain; mguc@irec.cat (M.G.); vizquierdo@irec.cat (V.I.-R.)

[*] Correspondence: jcuadra@uji.es

Abstract: In this study, ZnO/Ag nanocomposites were synthesized using a facile chemical route involving metallic precursors of zinc acetate dehydrate and silver acetate, and dissolving the two metallic precursors in EtOH. The final concentration of the solution was 0.4 M. The different nanocomposites were synthesized using different atomic percentages of silver to compare the amount of silver nanoparticles with the bactericidal power of the nanocomposites. They were prepared at concentrations of 0, 1, 3, 5, 7, and 10 at%. The as-prepared nanocomposites were characterized using X-ray diffraction (XRD), scanning electron microscopy (SEM) and scanning transmission electron microscopy (STEM) to study their structural and morphological properties. SEM showed that there is a clear effect of Ag on the size of the ZnO particles, since when silver percentages of 1 at% are included, the grain size obtained is much smaller than that of the ZnO synthesis. The effect is maintained for 3, 5, 7, and 10 at% silver. Transmission electron microscopy (TEM) compositional mapping confirms the presence of spherical nanoparticles in the synthesized samples. The size of the nanoparticles ranges from about 10 to about 30 nm. In addition, UV-Vis and Raman spectroscopy were performed to obtain structural details. The different samples show an increase in the absorption in the visible range due to the incorporation of the silver NPs. Measurement of the antimicrobial activity was tested against *Staphylococcus aureus* (*S. aureus*) and *Escherichia coli* (*E. coli*) It is shown that zinc oxide has bactericidal power for these two groups of bacteria and also that when it is used together with silver NP, this effect improves, eliminating more than 90% of inoculated bacteria.

Keywords: antimicrobial activity; Raman spectroscopy; nanocomposite; biomedical applications

1. Introduction

Metals have been used as antimicrobial agents since ancient times. For example, silver, copper, zinc, and arsenic have all been used to cure diseases caused by bacteria. Zinc and copper are associated with the mechanism by which pathogens are killed in eukaryotic cells, where oxidative stress is used to kill the engulfed microbe. Even low concentrations of metals such as gold, silver, and mercury are very toxic to bacteria and have broad-spectrum antibacterial actions [1,2]. Concerns about the safety of drug-resistant microbes and ongoing attention to the cost of healthcare have led to the focus being centered on replacing the traditional antimicrobial compounds or finding another alternative [3]. Polymeric structures characterized by antimicrobial properties have also aroused a great deal of interest in the scientific community, especially in areas such as food engineering (i.e., active packaging), and biomedical applications [4,5]. Nowadays, the interest in applying nanotechnology as an extremely powerful nano-weapon to solve this particular issue is increasing day by day. Microbes find it extremely difficult to survive against nanoparticles (NPs), as they target a wide range of different bacterial components, in sharp contrast to the mechanistic action of antibiotics [6].

Nano-hybrid crystals, especially metal oxides and rare earth oxides [7], have attracted special attention as they combine the properties of the constituent elements to produce a deeper and more synergistic effect, as in the case of the doping of structures using transition metals [8]. In recent years, zinc oxide (ZnO) has been recognized as a safe material by the U.S. Food and Drug Administration (21CFR182.8991; FDA, 2011), and the antibacterial activity of ZnO NPs has received a significant amount of interest worldwide particularly due to the implementation of nanotechnology to synthesize particles in the nanometer region [9]. ZnO NPs show great photocatalytic activity as they are an n-type II-VI semiconductor with a relatively large bandgap of ~3.3 eV and high excitation binding energy (~60 meV) at room temperature [10]. They also have good chemical stability as well as high temperature resistance (~1950 °C) in the hexagonal wurtzite structure [11]. ZnO maintains high optical absorption in the UVA (315–400 nm) and UVB (280–315 nm) regions, which is advantageous in antibacterial response because this feature significantly promotes the interaction of ZnO with bacteria [12–15]. ZnO is a more efficient photocatalyst than titanium dioxide (TiO_2) under visible light irradiation because it has greater quantum efficiency, lower cost of production, and higher biocompatibility than TiO_2 [16]. The photocatalytic activity can be modulated by allowing absorption in the visible range by introducing different types of dopants (metals or non-metals) [17,18]. Doping ZnO with noble metals such as gold (Au) and silver (Ag) has been reported to increase the photocatalytic activity of ZnO [19] because of improved charge separation and reduction in electron-hole recombination in ZnO [20]. The optical vibration of surface plasmon in metal nanoparticles enables absorption in the visible range (380–750 nm) and improves the photocatalytic activity of these metal–semiconductor composites under visible light [21]. Ag nanoparticles have been investigated by many researchers owing to this important role in a wide array of pathogens, particularly multi-resistant pathogens that are difficult to treat with the antibiotics currently available [22]. The most commonly used bacteria to test the bactericidal effect of nanoparticles of different compositions are *S. aureus* and *E. coli* [3,23,24]. *S. aureus* is a Gram-positive bacterium, with a high content of peptidoglycan in the cell wall. It is able to survive in variable environmental conditions, such as low pH or starvation. It is considered an important human pathogen that can cause severe skin infections or internal infections when it breaks through defensive barriers. *E. coli* is a Gram-negative bacterium, the cell wall of which has a totally different structure from Gram-positive bacteria since it is surrounded by a lipidic membrane on the outside. It is a bacterium that indicates fecal contamination, as it is present in intestinal microbiota. Although many strains are harmless, there are several highly dangerous species such as enterotoxigenic and enterohaemorrhagic varieties. Both bacteria can acquire resistance to antibiotics, and in this way become more hazardous [24]. Therefore, controlling the growth of these bacteria is important for human health.

The effect that Ag NPs might have on bacteria has been explored in different studies, either to enhance the effectiveness of certain antibiotics [25] or against selected Gram-negative foodborne pathogens [26]. A review of this previous research shows that different methods of synthesis of NPs, as well as different methods to determine the antimicrobial activity, are used, thereby making it difficult to compare the results obtained by different authors.

The present work aims to determine the ability of the ZnO/Ag nanocomposites to inhibit or to reduce bacterial growth by using a novel synthesis based on the sol-gel methodology for the generation of ZnO/Ag nanocomposites. In addition, their characterization using Raman spectroscopy is a very innovative and profound advance in the field. The antimicrobial power is also measured in two different types of bacteria, demonstrating important antimicrobial properties in these nanocomposites that allow them to be used as powerful antimicrobial agents.

2. Materials and Methods

2.1. Synthesis of ZnO/Ag Nanocomposites

ZnO/Ag nanocomposites were prepared by the sol-gel method. The solutions were prepared using metallic precursors of zinc acetate dihydrate ($C_4H_6O_4Zn\cdot H_2O$, Sigma-

Aldrich, Steinheim, Germany, >99%) and silver acetate ($C_2H_3AgO_2$, Sigma-Aldrich). These ZnO/Ag nanocomposites were prepared with concentrations of 0, 1, 3, 5, 7, and 10 at% of silver, labeled Zn1, Zn2, Zn3, Zn4, Zn5, and Zn6. The concentration of the final solutions was 0.4 M.

The first step of sol-gel synthesis is based on dissolving the two metallic precursors in 20 mL of ethanol (EtOH, Scharlau, Sentmenat, Spain) using a magnetic stirrer at room temperature (25 °C). After preparation, triethanolamine ($C_6H_{15}NO_3$, Acros Organics, Spain, Barcelona, 99%) was added to the solution as a reducing/precipitation agent. After approximately 30 min stirring at room temperature, a dense white gel was formed. We let it dry for 30 min at room temperature before the gel was calcined at 600 °C for 1 h in a muffle furnace to obtain white-colored nanopowders as the final product (Scheme 1).
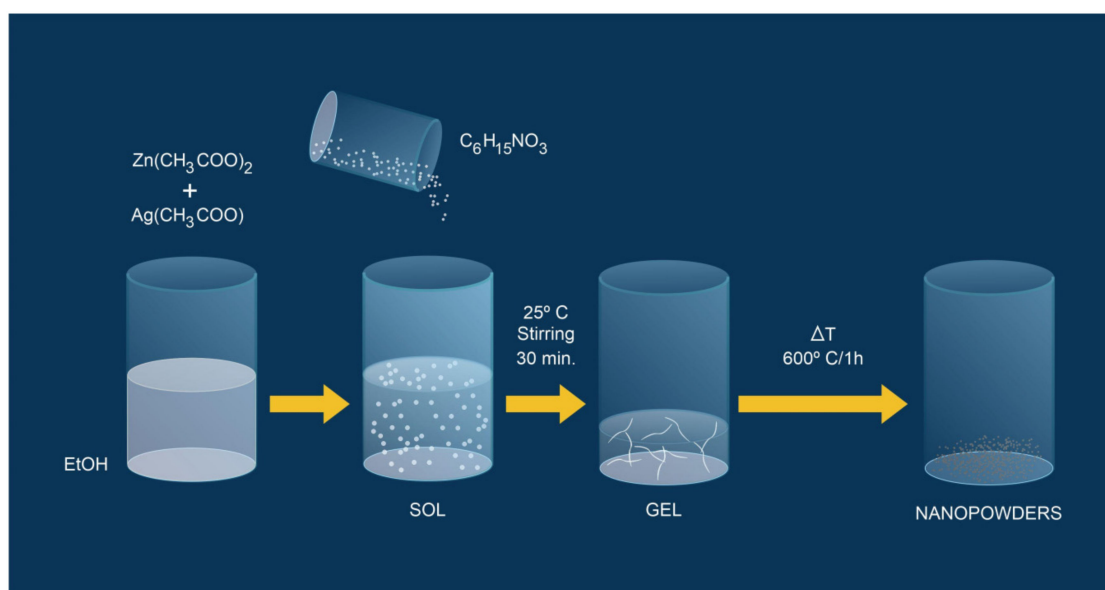
Scheme 1. The synthesis of the antimicrobial ZnO/Ag nanocomposites.

2.2. Characterization

The crystal structures of the different ZnO/Ag nanocomposite samples were studied using X-ray diffraction (XRD) measurements. To do so, an X-ray diffractometer (D4 Endeavor, Burker-ASX) equipped with a Cu Kα radiation source was used. Data was collected by step-scanning from 10° to 80° with a step size of 0.05°/2θ and 5 s counting time per step. The morphology and the size of the ZnO/Ag nanocomposites were observed using a JEOL JEM-1010 200 kV Field Emission Transmission Electron Microscope (TEM 200) equipped with a JEOL EM-24830FLASH digital camera with a CMOS sensor, offering a resolution of 2 k × 2 k. The maximum resolution achieved was 0.23 nm. The microscope was also equipped with a STEM DF/BF image acquisition system with a resolution of 1 nm and an Aztec TEM Ultim Max microanalysis system from Oxford with a drift silicon sensor without a window of 80 mm^2 and a resolution of 127 eV for the Mn Kα line.

Raman scattering measurements were performed using a Hobiba Jobin-Yvon FHR-640 monochromator coupled with a CCD detector in backscattering configuration through a specific probe designed at the Catalonia Institute for Energy Research (IREC). The spectra were excited by gas (325 nm) with a density power of ~10 W/cm^2. Calibration of the spectral position was performed by imposing the main peak of single-crystalline Si to 520 cm^{-1}. For each sample, the measurements were carried out at 9 points with a laser spot diameter of ~70 μm, which made it possible to exclude the local variations due to different crystalline orientations of the grains and possible inhomogeneities between specific grains. UV–visible (UV-Vis) diffuse reflectance spectroscopy of the samples was performed to

study the optical properties of the ZnO/Ag nanocomposites using a CARY 500 SCAN VARIAN spectrophotometer in the 220–600 nm range. BaSO4 was used as a reference.

2.3. Bactericidal Test of ZnO/Ag Nanocomposites

The antimicrobial effect of the ZnO/Ag nanocomposites was tested against the *S. aureus* ATCC 29213 and the *E. coli* NCIMB 9484 strains, both from the Spanish Type Culture Collection (CECT).

The strains were pre-cultivated on Luria Bertani (LB) agar plates at 37 °C to obtain the inoculum. After 24 h, the bacteria were harvested in sterilized $MgSO_4$ (10 mM). LB supplemented with ZnO or ZnO/Ag nanocomposites was used in the bacterial growth assays.

The growth assays were carried out in a Multiskan FCMicroplate Photometer (Thermo Scientific, Waltham, MA, USA) with a total volume of 200 μL in microlitre wells using an initial bacterial density of 10^6 cfu mL^{-1} of *S. aureus* and 10^5 cfu mL^{-1} of *E. coli*. Bacterial growth was incubated at 37 °C with continuous agitation and monitored by measuring the optical density every 10 min with periodic shaking for 24 h. The results were printed out as growth curves.

To test whether the applied nanocomposites had an antimicrobial or bacteriostatic effect, live and dead cell quantification was used. The proportion of living vs. dead cells was quantified using the fluorescent LIVE/DEAD BacLight Bacterial Viability Kit, L13152 (Molecular Probes, Invitrogen, Paisley, UK). For live and dead cell quantification, 50 microL of bacterial suspension was mixed with 25 microL of each of the two components of the LIVE/ DEAD BacLight kit and incubated in the dark for 20 min. Then, the ratio of live/dead cells was determined by flow cytometric analysis. Samples were analyzed on a Becton Dickinson FACScan flow cytometer using the CellQuest software, which was also used to determine the percentage of live/dead cells. SYTO9 (Live) was excited at 480 nm and fluorescence was analyzed at 500 nm, whereas Propidium Iodide (Dead) was excited at 490 nm and fluorescence analyzed at 635 nm.

Statistical analysis was carried out using a one-way analysis of variance in the Statgraphics-plus software of Windows V.5 (Statistical Graphics Corp., Rockville, MD, USA). The means were expressed with standard errors and compared using a Fisher's least-significant difference test at the 95% confidence interval. Each experiment consisted of eight technical repetitions which were repeated three times.

3. Results and Discussion

3.1. Characterization of ZnO/Ag Nanocomposites

3.1.1. XRD Analysis

The crystalline behavior and structural properties of ZnO/Ag nanocomposites were revealed by powder XRD measurements. XRD patterns of the samples were prepared by means of concentrations of 0, 1, 3, 5, 7, and 10 at% of silver are shown in Figure 1. The diffraction patterns obtained were analyzed by X'Pert High Score Plus software. The diffraction peaks are all very sharp, which reflects a polycrystalline with good crystallinity. It was observed that when the Ag at% is raised, the intensity of the diffraction peaks corresponding to the cubic structure of Ag NPs (PDF No. 03-065-2871, a = 4.09 Å) increases the crystallinity. The three diffraction peaks at 2θ of 38.1°, 44.3°, and 64.4° correspond to the crystal planes of (100), (200), and (220), respectively. ZnO peaks corresponding to a hexagonal wurtzite structure (PDF No. 01-080-0074, a = 3.25 Å, c = 5.21 Å) remained stable for all the concentrations. The eight diffraction peaks belonging to ZnO were at 2θ of 31.7°, 34.3°, 36.2°, 47.4°, 56.5°, 62.7°, 67.8°, and 68.9°, which correspond to the crystal planes of (100), (002), (101), (102), (110), (103), (112), and (201), respectively. However, the XRD patterns indicate the formation of separate phases, a hexagonal wurtzite structure for ZnO, and a cubic structure for Ag NPs. The formation of these separate phases can be seen when the atomic percentage of silver surpassed a value of 3%. No other peaks were identified, suggesting the purity of the synthesized samples
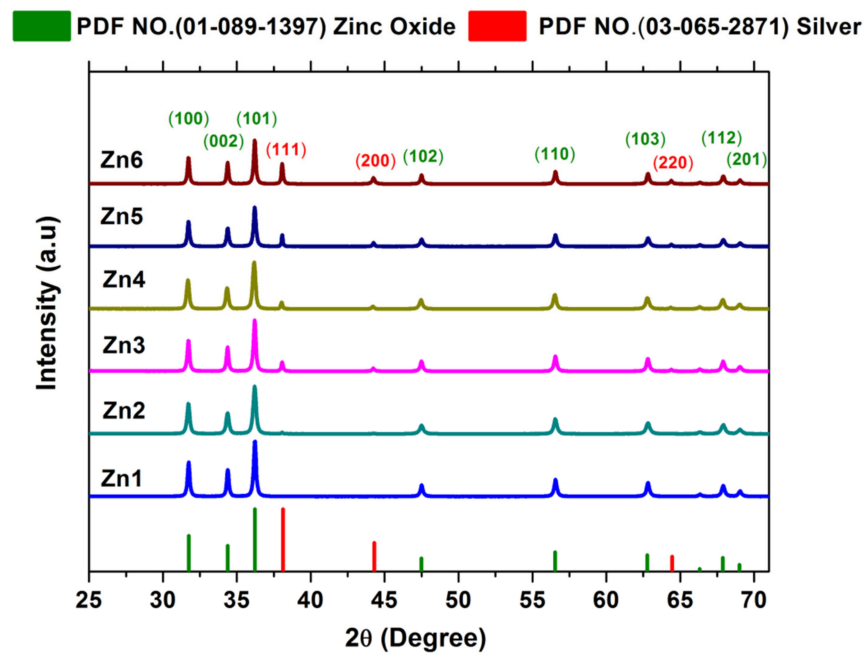
Figure 1. XRD patterns for the different silver concentrations of the nanocomposites (Zn1, Zn2, Zn3, Zn4, Zn5, and Zn6).

3.1.2. Morphological, Size, and Compositional Analysis of ZnO/Ag Nanocomposites

The SEM images of the synthesized ZnO/Ag nanocomposites are shown in Figure 2. Figure 2a displays the agglomerated particles of pure ZnO. Figure 2a–f shows the samples prepared by means of concentrations of 0, 1, 3, 5, 7, and 10 at% of silver. The effect of Ag on the size of ZnO particles is clear. In Figure 2a, with 0% Ag, there are both small and big particles. After adding 1% Ag (Figure 2b), all the grains are small, which should be the best sample for antibacterial purposes, as they have a higher surface/volume ratio. Increasing the amount of Ag only decreases the number of small particles, so they almost disappear in samples with 7% (Figure 2e) and 10% (Figure 2f). In this way, an increase in the amount of Ag by more than 5% varies the particle size, causing the surface/volume ratio to decrease considerably. The size of the Ag particles was very small (<30 nm), and for this reason, transmission electron microscopy (TEM) was used to evaluate the particle size and composition of the Ag nanoparticles.

STEM allows determination of the shape and particle size distribution of the silver nanoparticles and their location on the nanocomposite. Figure 3 shows selected STEM images and the element mapping of the ZnO/Ag nanocomposites. The STEM image (Figure 3a) shows the presence of the Ag nanoparticles on the zinc oxide, thus forming the ZnO/Ag nanocomposite, which corresponds to sample Zn1 (1 at% of Ag). The Ag nanoparticles are mostly deposited in spherical form on the surface of the zinc oxide. The size of the silver nanoparticles ranged between 10 and 30 nanometers. The distribution map of Zn (Figure 3b) was collected using Kα X-rays. Figure 3c shows the distribution map of O using Kα X-rays. The Ag map in Figure 3d also consists of Kα X-rays. The Ag maps can be observed even for some small particles. It is clear that in the case of the Ag nanoparticles shown here, the Ag signals are distributed in different regions as Zn signals or O signals, perfectly indicating the position of the Ag nanoparticles.
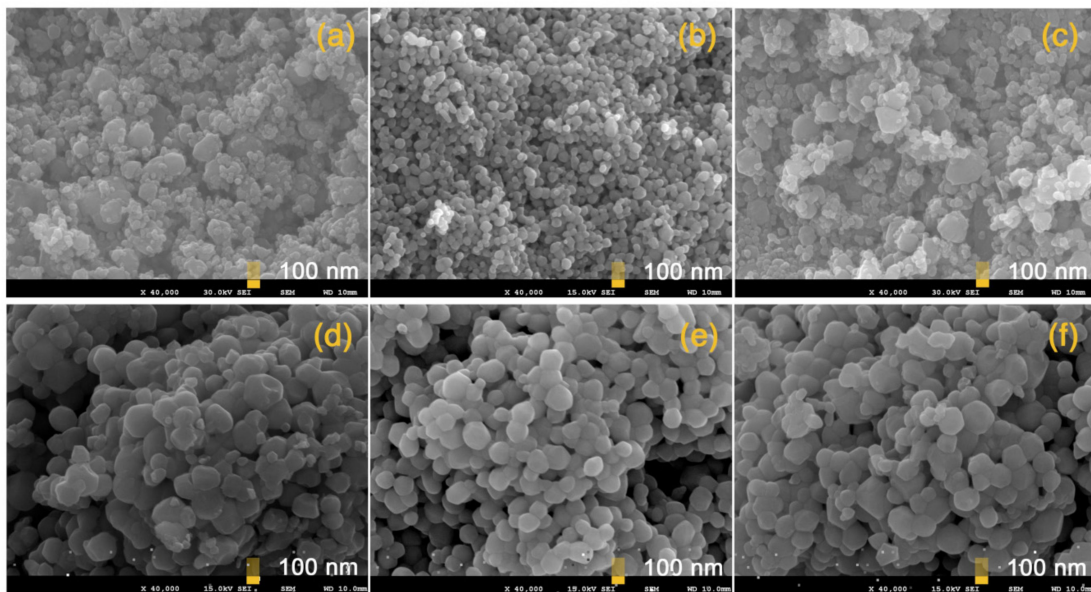
Figure 2. SEM images of ZnO/Ag nanocomposites: (**a**) Zn1, (**b**) Zn2, (**c**) Zn3, (**d**) Zn4, (**e**) Zn5, and (**f**) Zn6.
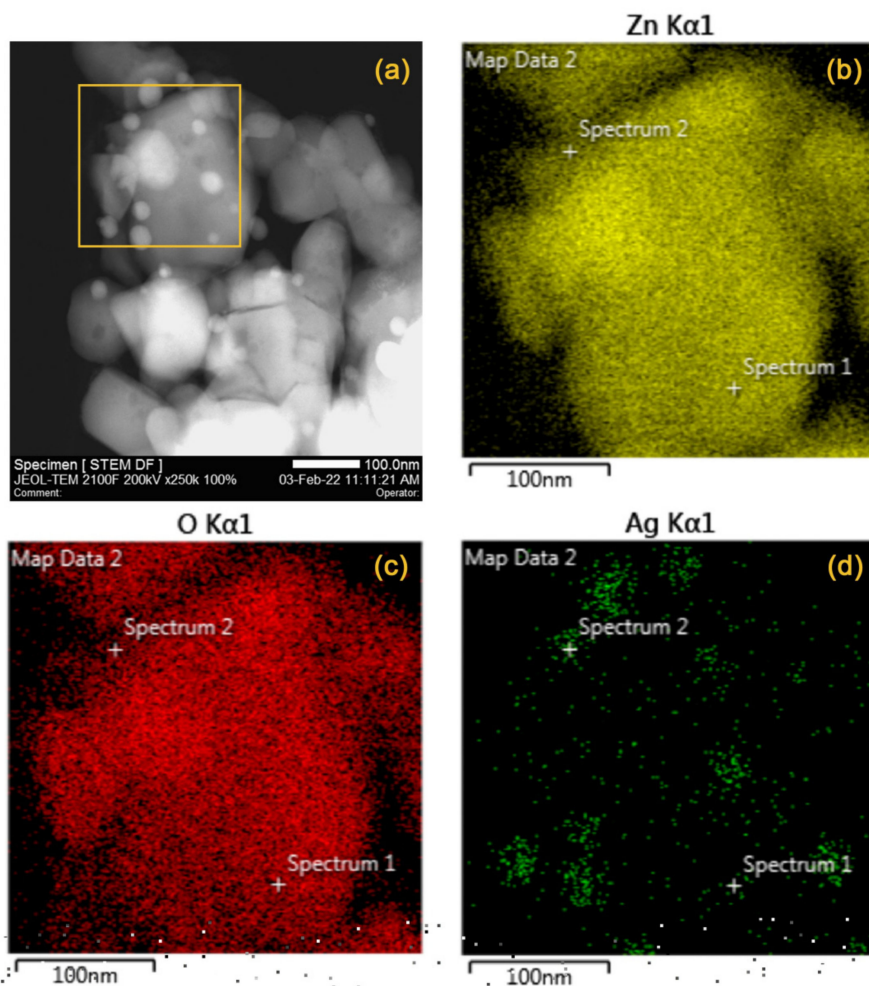

Figure 3. (**a**) STEM images of ZnO/Ag nanocomposites; (**b**) Elemental mapping of Zn collected using Kα X-rays, (**c**) Elemental mapping of O collected using Kα X-rays; (**d**) Elemental mapping of Ag collected using Kα X-rays.

3.1.3. UV-Vis Spectroscopy Studies

The absorption properties of ZnO/Ag nanocomposites were investigated with UV-Vis spectroscopy in the 200–650 nm range of wavelengths. Figure 4 shows the absorption spectra for Ag nanoparticles on ZnO with different atomic contents of Ag. All the samples show strong absorption in the UV range. Additionally, the broad exciton-related peak at 360–370 nm disappears, and this behavior is associated with UV absorption in zinc oxide [27]. The absorption spectrum of pure ZnO shows maximum absorption at 360 nm. Furthermore, with the Zn2 sample, the absorption edge shifted to a higher wavelength (365 nm) with respect to pure ZnO (Zn1). This shift is related to the incorporation of Ag NPs in the ZnO matrix [28].
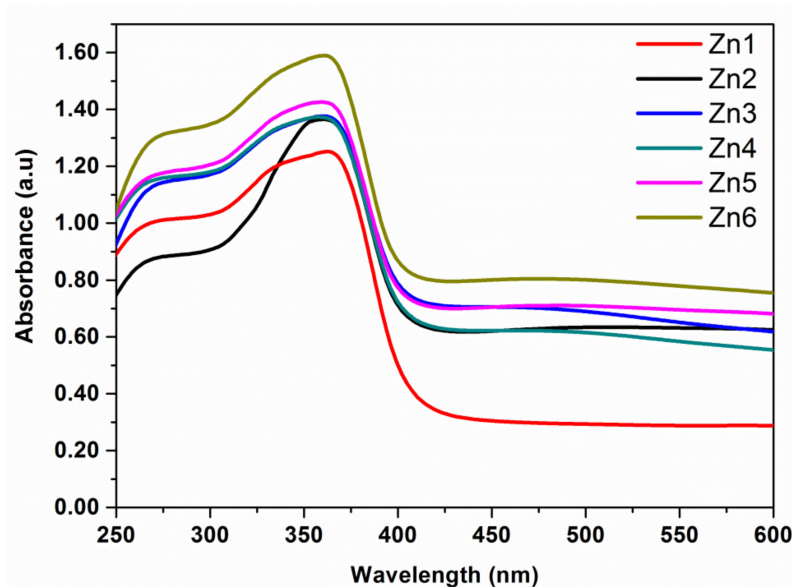

Figure 4. Absorption spectra of ZnO/Ag Nanocomposites: Zn1, Zn2, Zn3, Zn4, Zn5, and Zn6.

3.1.4. Raman Spectroscopy

Spectra measured under the 325 nm excitation wavelength are presented in Figure 5, which shows the typical spectra of ZnO compounds under the resonant conditions, with an intense LO peak (sum of two modes with A1 (LO) and E1 (LO) symmetry) and its second-order 2LO peak [29]. In the average spectra of each sample, additional small intensity peaks can be identified (see the vertical dashed lines in Figure 6). All of them are related to the fundamental or previously observed multiphonon modes of the ZnO compound [30]. No additional peaks/bands that can be associated with the presence of Ag NPs in the powders can be observed in the spectra that were measured.

Furthermore, the homogeneity of the samples and possible correlation of the Ag atomic percentage with the intensity of additional peaks/bands were accomplished. For this different reference, the LO peak in the spectra was selected, measured under 325 nm excitation. This peak is separated from the additional bands and makes it possible to define the homogeneity or correlate the spectra evolution with the Ag content. The homogeneity of the powders was assessed by calculating the relative integrated intensity of the 2LO peak in the spectra measured under 325 nm excitation. The ratio of intensities between the 2LO and LO peaks mainly changes due to the band gap variation in the ZnO compound, which changes the proximity to the resonant conditions [31,32]. As seen from the box plot in the left panel of Figure 6, the mean value of the relative integrated intensity of the 2LO peak is quite similar in all the samples, except for sample Zn4. Also, the homogeneity of the samples is different and is can be seen to be quite good for Zn2, with Zn3 being the worst. No correlation of the mean value or the inhomogeneity of the sample with the amount of Ag concentration was observed, assuming a gradual increase in the Ag NPs in the nanocomposites from sample Zn1 to sample Zn6.
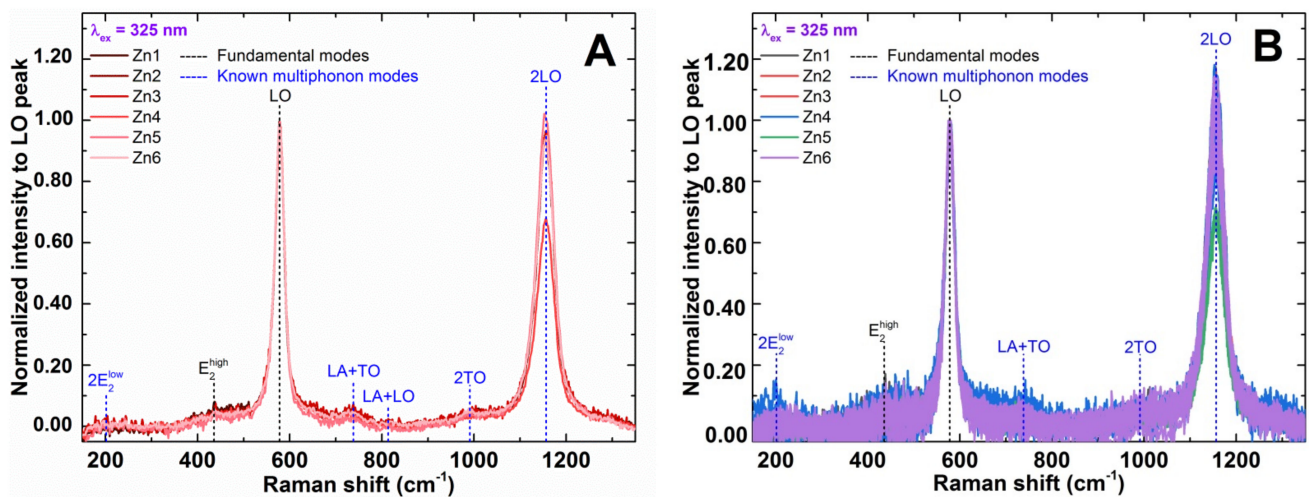
Figure 5. (**A**) Raman scattering spectra of nanocomposite samples (Zn1, Zn2, Zn3, Zn4, Zn5, and Zn6) were measured under 325 nm excitation wavelength in different points of the samples and (**B**) averaged per sample.
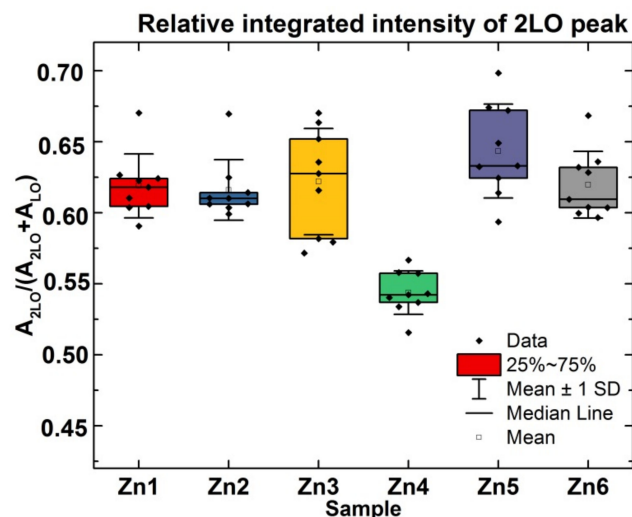

Figure 6. Relative integrated intensity of 2LO peak from the spectra measured under 325 nm excitation wavelength.

3.2. Antimicrobial Activity of ZnO/Ag Nanocomposites

The effect of ZnO/Ag nanocomposites at different concentrations of Ag was analyzed in vitro against *S. aureus* and *E. coli*. The results showed a reduction in the growth of both bacteria in the presence of ZnO and ZnO/Ag nanocomposites when compared to controls. The antimicrobial effect of ZnO nanoparticles has been previously demonstrated, with an increase in the action of some antibiotics being observed in the presence of NP [33,34].

In the same way, there is clear evidence that the use of Ag nanoparticles increases the antimicrobial effect of certain antibiotics or defense-inducing molecules such as chitosan, which makes it difficult to analyze the effect of the nanoparticles [13,23,35–37]. Other authors have tested in vitro the effects of Ag NPs against *E. coli* and *S. aureus*, noting that Ag NPs were effective against *E. coli* but not against *S. aureus*. However, the mechanism of action of the Ag NPs is still unknown, since it depends on the type of nanoparticle, the size, the arrangement of the ions, and their concentration [14,34,38,39] as well as the morphology of the bacteria (type of cell wall, type of metabolism, virulence mechanism, etc.) [40]. Previous studies have suggested that the action of Ag NPs on bacteria may be due to their ability to penetrate the cell [41], the production of reactive oxygen species

(ROS) [42], or the formation of free radicals, as well as the inactivation of proteins in the cell by silver ions [15].

The variability of these results led us to test the effect of ZnO combined with different concentrations of silver on *E. coli* and *S. aureus*. The novelty of our study lies in the synthesis method of the AgNPs, which is a novel synthesis method based on sol-gel methodology, and in the fact that AgNPs synthized in this study were able to inhibit high concentrations of both bacteria, which rarely occurs in real-life systems. The results obtained are shown in Figure 7.
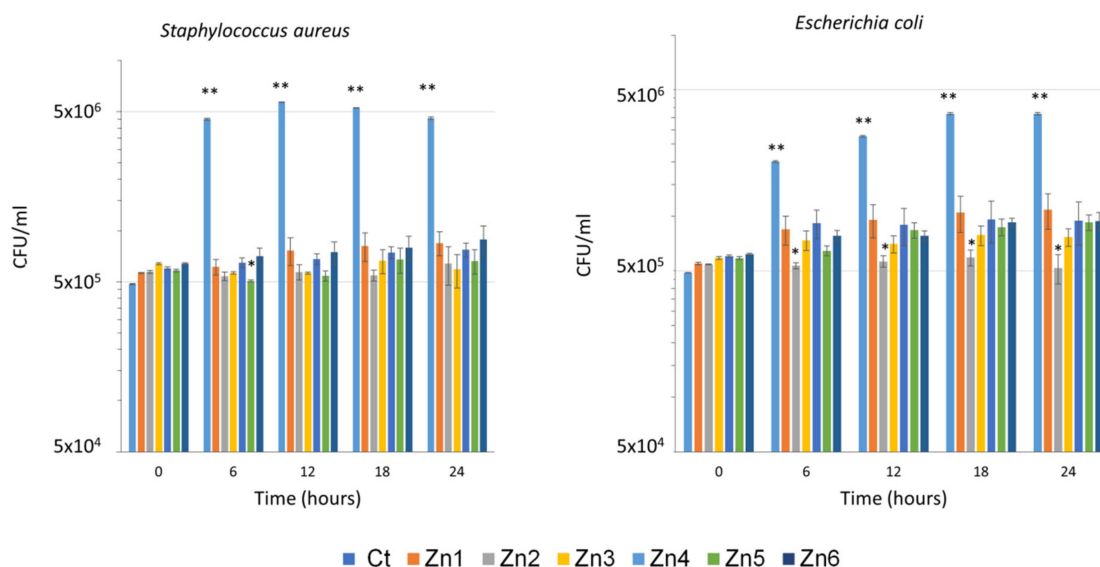

Figure 7. Results of the effect of the treatments on *S. aureus* and *E. coli* in the absence of treatment (Ct), with ZnO (Zn1) and with the ZnO/Ag nanocomposites (Zn2, Zn3, Zn4, Zn5, and Zn6). The bars on the graphs represent the standard error; the asterisks indicate significant differences.

Under our conditions, a reduction in bacterial growth was observed from 3 h of inoculation in both bacteria and all treatments when compared to the control. In *S. aureus*, a similar effect in growth inhibition was observed in ZnO with or without Ag NPs; in *E. coli*, bacterial growth was greater in the absence of Ag NPs at all sampling times, although no significant differences were observed (Figure 8). These results are in concordance with previous works observing that Gram-negative bacteria are more susceptible to silver nanoparticles. This may be due to the fact that the cellular wall of Gram-negative bacteria is narrower than that of Gram-positive strains, which may reduce the penetration of nanoparticles into the bacterial cells [43]. When analyzing the effect of the different concentrations of Ag against both bacteria, it can be seen that an increase in the concentration of Ag does not correlate with an increase in its effect against the bacteria. Furthermore, it seems that lower concentrations of Ag have greater efficacy against *E. coli*.

In order to check whether the effect of the Zn/Ag nanocomposites was bacteriostatic or bactericidal, the samples were stained with the LIVE/DEAD BacLight kit and further analyzed through flow cytometry. All treatments showed a bactericidal effect when compared to controls, as seen in Figure 8. The treatments reduced the percentage of living cells by more than 90% in most cases. Table 1 shows the results of the percentages of live bacteria concerning the total number of cells counted, which were obtained using the flow cytometer after being stained with the live/dead kit.
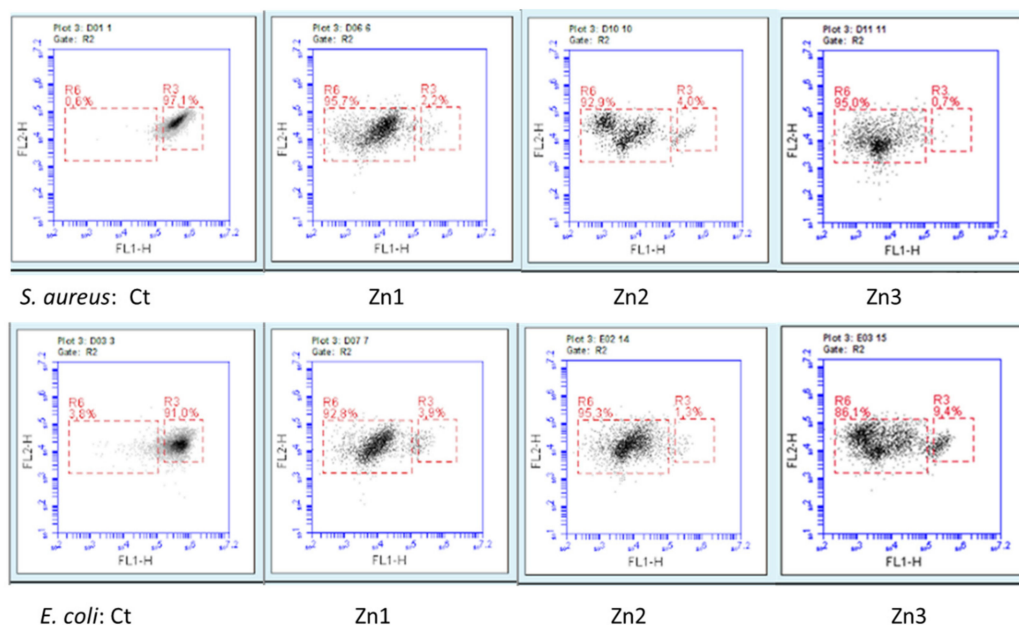
Figure 8. Cytometry charts showing the percentage of live and dead cells.

Table 1. Percentage of live bacteria determined by using the flow-cytometer after being stained with the live/dead kit.

	Name of Sample	Ctr	Zn1	Zn2	Zn3	Zn4	Zn5	Zn6
Percentage of	*S. aureus*	96.5	15	9	9	9	8	9
live bacteria (%)	*E. coli*	91.25	12	6	6.5	9.5	5.5	4.5

The fact that increasing the silver concentration does not correlate with an increase in its antibacterial effect could be due to the arrangement of Ag in the NPs when added at higher concentrations. At higher concentrations, Ag tends to agglomerate, thereby decreasing the area of its surface in contact with the bacteria. Moreover, at higher concentrations of Ag, the size of the NPs is larger, as shown in Figure 2. Related to this, Ref. [44] reported that AgNPs of smaller size could cause more toxicity to the bacteria and show better bactericidal effects compared to the larger particles as they have larger surface area. In addition to being able to penetrate into bacterial cells, it is thought that another mechanism by which Ag NPs are killing bacteria is by releasing silver ions [45]. The efficiency of this process depends on different factors, such as intrinsic AgNP characteristics and surrounding media. For example, smaller silver nanoparticles are more prone to Ag release, due to their larger surface area. These findings could also support the fact that in our results, the antibacterial effect is not correlated with the concentration of Ag since Zn2 NPs containing 1% Ag are the smallest and are the most effective against the tested bacteria.

4. Conclusions

In summary, a soft chemical route was performed to prepare ZnO/Ag nanocomposites. The XRD patterns indicate the formation of separate phases, namely, a hexagonal wurtzite structure for ZnO and a cubic structure for Ag NPs. The formation of these separate phases can be seen when the atomic percentage of silver exceeds 3%. SEM shows that the presence of these Ag nanoparticles causes the growth of ZnO to vary, which can then affect its bactericidal power. STEM allows the morphology and sizes of the Ag NPs to be nano-spheres (~20 nm) on the wurtzite ZnO surface. The absorption bands from the UV-Vis analysis of the samples increase due to the contribution from the surface plasmon resonance absorption of silver nanoparticles, showing significantly higher visible light absorption compared to the ZnO matrix. Raman spectroscopy showed that spectra

measured in non-resonant conditions displayed a clear difference between the ZnO powder (Zn1) and nanocomposites with different Ag concentrations (Zn2–Zn6). Here, several non-fundamental peaks/bands are activated after adding Ag. In this way, it is clear that the silver is segregated in the form of NP and does not occupy positions within the zinc oxide structure. Some of them can be assigned to the previously observed multiphonon modes. When analyzing the effect of the different concentrations of Ag against both bacteria, we can observe that an increase in the concentration of Ag does not correlate with an increase in its effect against the bacteria. Consequently, when the percentage of dopant increases, the Ag NPs tend to agglomerate, thereby decreasing both their surface area and the area of their surface in contact with the bacteria. Hence, using only 1 at% of Ag reduces the percentage of living cells by more than 90% in most cases, thus increasing their effectiveness in the destruction of bacteria by 5% compared to that of zinc oxide without Ag NPs.

References

1. Lara, H.H.; Garza-Treviño, E.N.; Ixtepan-Turrent, L.; Singh, D.K. Silver nanoparticles are broad-spectrum bactericidal and virucidal compounds. *J. Nanobiotechnol.* **2011**, *9*, 2–9. [CrossRef] [PubMed]
2. Mittapally, S.; Taranum, R.; Parveen, S. Metal ions as antibacterial agents. *J. Drug Deliv. Ther.* **2018**, *8*, 411–419. [CrossRef]
3. Kim, J.S.; Kuk, E.; Yu, K.N.; Kim, J.-H.; Park, S.J.; Lee, H.J.; Kim, S.H.; Park, Y.K.; Park, Y.H.; Hwang, C.-Y.; et al. Antimicrobial effects of silver nanoparticles. *Nanomed. Nanotechnol. Boil. Med.* **2007**, *3*, 95–101. [CrossRef] [PubMed]
4. Baldino, L.; Aragón, J.; Mendoza, G.; Irusta, S.; Cardea, S.; Reverchon, E. Production, characterization and testing of antibacterial PVA membranes loaded with HA-Ag$_3$PO$_4$ nanoparticles, produced by SC-CO$_2$ phase inversion. *J. Chem. Technol. Biotechnol.* **2018**, *94*, 98–108. [CrossRef]
5. Huang, S.-M.; Liu, S.-M.; Ko, C.-L.; Chen, W.-C. Advances of Hydroxyapatite Hybrid Organic Composite Used as Drug or Protein Carriers for Biomedical Applications: A Review. *Polymers* **2022**, *14*, 976. [CrossRef]
6. Matai, I.; Sachdev, A.; Dubey, P.; Kumar, S.U.; Bhushan, B.; Gopinath, P. Antibacterial activity and mechanism of Ag–ZnO nanocomposite on *S. aureus* and GFP-expressing antibiotic resistant *E. coli*. *Colloids Surf. B Biointerfaces* **2014**, *115*, 359–367. [CrossRef]
7. Hossain, M.K.; Khan, M.I.; El-Denglawey, A. A review on biomedical applications, prospects, and challenges of rare earth oxides. *Appl. Mater. Today* **2021**, *24*, 101104. [CrossRef]
8. Okeke, I.S.; Agwu, K.K.; Ubachukwu, A.A.; Ezema, F.I. Influence of transition metal doping on physiochemical and antibacterial properties of ZnO[sbnd] Nanoparticles: A review. *Appl. Surf. Sci. Adv.* **2022**, *8*, 100227. [CrossRef]
9. Sirelkhatim, A.; Mahmud, S.; Seeni, A.; Kaus, N.H.M.; Ann, L.C.; Bakhori, S.K.M.; Hasan, H.; Mohamad, D. Review on Zinc Oxide Nanoparticles: Antibacterial Activity and Toxicity Mechanism. *Nano-Micro Lett.* **2015**, *7*, 219–242. [CrossRef]
10. Saoud, K.; Alsoubaihi, R.; Bensalah, N.; Bora, T.; Bertino, M.; Dutta, J. Synthesis of supported silver nano-spheres on zinc oxide nanorods for visible light photocatalytic applications. *Mater. Res. Bull.* **2015**, *63*, 134–140. [CrossRef]
11. Djurišić, A.B.; Leung, Y.H. Optical Properties of ZnO Nanostructures. *Small* **2006**, *2*, 944–961. [CrossRef] [PubMed]
12. Azfar, A.K.; Kasim, M.F.; Lokman, I.M.; Rafaie, H.A.; Mastuli, M.S. Comparative study on photocatalytic activity of transition metals (Ag and Ni)-doped ZnO nanomaterials synthesized via sol–gel method. *R. Soc. Open Sci.* **2020**, *7*, 191590. [CrossRef] [PubMed]

13. Wolny-Kołądka, K.; Lenart-Boroń, A. Antimicrobial resistance and the presence of extended-spectrum beta-lactamase genes in Escherichia coli isolated from the environment of horse riding centers. *Environ. Sci. Pollut. Res.* **2018**, *25*, 21789–21800. [CrossRef] [PubMed]

14. Meier, M.J.; Dodge, A.E.; Samarajeewa, A.D.; Beaudette, L.A. Soil exposed to silver nanoparticles reveals significant changes in community structure and altered microbial transcriptional profiles. *Environ. Pollut.* **2020**, *258*, 113816. [CrossRef] [PubMed]

15. Rai, M.; Kon, K.; Ingle, A.; Duran, N.; Galdiero, S.; Galdiero, M. Broad-spectrum bioactivities of silver nanoparticles: The emerging trends and future prospects. *Appl. Microbiol. Biotechnol.* **2014**, *98*, 1951–1961. [CrossRef]

16. Zhang, J. Silver-coated Zinc Oxide Nanoantibacterial Synthesis and Antibacterial Activity Characterization. In Proceedings of the 2011 International Conference on Electronics and Optoelectronics, Dalian, China, 29–31 July 2011; pp. V3-94–V3-98.

17. Kamat, P.V.; Huehn, R.; Nicolaescu, R. A "Sense and Shoot" Approach for Photocatalytic Degradation of Organic Contam-inants in Water. *J. Phys. Chem. B* **2002**, *106*, 788–794. [CrossRef]

18. Herrmanna, J.; Lassalettac, G.; Fernbdez, A. Characterization and photocatalytic activity in aqueous medium of Ti02 and Ag-Ti02 coatings on quartz. *Appl. Catal. B Environ.* **1997**, *13*, 219–228. [CrossRef]

19. Karunakaran, C.; Rajeswari, V.; Gomathisankar, P. Enhanced photocatalytic and antibacterial activities of sol–gel synthesized ZnO and Ag-ZnO. *Mater. Sci. Semicond. Process.* **2011**, *14*, 133–138. [CrossRef]

20. Merga, G.; Cass, L.C.; Chipman, D.M.; Meisel, D. Probing Silver Nanoparticles During Catalytic H2 Evolution. *J. Am. Chem. Soc.* **2008**, *130*, 7067–7076. [CrossRef]

21. Stathatos, E.; Petrova, T.; Lianos, P. Study of the Efficiency of Visible-Light Photocatalytic Degradation of Basic Blue Adsorbed on Pure and Doped Mesoporous Titania Films. *Langmuir* **2001**, *17*, 5025–5030. [CrossRef]

22. Gajbhiye, M.; Kesharwani, J.; Ingle, A.; Gade, A.; Rai, M. Fungus-mediated synthesis of silver nanoparticles and their activity against pathogenic fungi in combination with fluconazole. *Nanomed. Nanotechnol. Biol. Med.* **2009**, *5*, 382–386. [CrossRef] [PubMed]

23. Shahverdi, A.R.; Fakhimi, A.; Shahverdi, H.R.; Minaian, S. Synthesis and effect of silver nanoparticles on the antibacterial activity of different antibiotics against Staphylococcus aureus and *Escherichia coli*. *Nanomed. Nanotechnol. Biol. Med.* **2007**, *3*, 168–171. [CrossRef] [PubMed]

24. Gouyau, J.; Duval, R.; Boudier, A.; Lamouroux, E. Investigation of Nanoparticle Metallic Core Antibacterial Activity: Gold and Silver Nanoparticles against *Escherichia coli* and *Staphylococcus aureus*. *Int. J. Mol. Sci.* **2021**, *22*, 1905. [CrossRef] [PubMed]

25. Aymonier, C.; Schlotterbeck, U.; Antonietti, L.; Zacharias, P.; Thomann, R.; Tiller, J.C.; Mecking, S. Hybrids of silver nanoparticles with amphiphilic hyperbranched macromolecules exhibiting antimicrobial properties. *Chem. Commun.* **2002**, *24*, 3018–3019. [CrossRef] [PubMed]

26. Loo, Y.Y.; Rukayadi, Y.; Nor-Khaizura, M.-A.; Kuan, C.H.; Chieng, B.W.; Nishibuchi, M.; Radu, S. In Vitro Antimicrobial Activity of Green Synthesized Silver Nanoparticles Against Selected Gram-negative Foodborne Pathogens. *Front. Microbiol.* **2018**, *9*, 1555. [CrossRef]

27. Goh, E.; Xu, X.; McCormick, P. Effect of particle size on the UV absorbance of zinc oxide nanoparticles. *Scr. Mater.* **2014**, *78–79*, 49–52. [CrossRef]

28. Singh, R.; Barman, P.B.; Sharma, D. Synthesis, structural and optical properties of Ag doped ZnO nanoparticles with enhanced photocatalytic properties by photo degradation of organic dyes. *J. Mater. Sci. Mater. Electron.* **2017**, *28*, 5705–5717. [CrossRef]

29. Phan, T.-L.; Vincent, R.; Cherns, D.; Dan, N.H.; Yu, S.-C. Enhancement of multiple-phonon resonant Raman scattering in Co-doped ZnO nanorods. *Appl. Phys. Lett.* **2008**, *93*, 082110. [CrossRef]

30. Cuscó, R.; Alarcón-Lladó, E.; Ibáñez, J.; Artús, L.; Jiménez, J.; Wang, B.; Callahan, M.J. Temperature dependence of Raman scattering inZnO. *Phys. Rev. B* **2007**, *75*, 165202. [CrossRef]

31. Rousset, J.; Saucedo, E.; Lincot, D. Extrinsic Doping of Electrodeposited Zinc Oxide Films by Chlorine for Transparent Conductive Oxide Applications. *Chem. Mater.* **2009**, *21*, 534–540. [CrossRef]

32. Guc, M.; Tsin, F.; Rousset, J.; Romanyuk, Y.E.; Izquierdo-Roca, V.; Pérez-Rodríguez, A. Nondestructive Raman Scattering Assessment of Solution-Processed ZnO-Doped Layers for Photovoltaic Applications. *J. Phys. Chem. C* **2017**, *121*, 3212–3218. [CrossRef]

33. Banoee, M.; Seif, S.; Nazari, Z.E.; Jafari-Fesharaki, P.; Shahverdi, H.R.; Moballegh, A.; Moghaddam, K.M.; Shahverdi, A.R. ZnO nanoparticles enhanced antibacterial activity of ciprofloxacin against Staphylococcus aureus and *Escherichia coli*. *J. Biomed. Mater. Res. Part B Appl. Biomater.* **2010**, *93*, 557–561. [CrossRef] [PubMed]

34. Chakraborti, S.; Mandal, A.; Sarwar, S.; Singh, P.; Chakraborty, R.; Chakrabarti, P. Bactericidal effect of polyethyleneimine capped ZnO nanoparticles on multiple antibiotic resistant bacteria harboring genes of high-pathogenicity island. *Colloids Surf. B Biointerfaces* **2014**, *121*, 44–53. [CrossRef] [PubMed]

35. Fayaz, A.M.; Balaji, K.; Girilal, M.; Yadav, R.; Kalaichelvan, P.T.; Venketesan, R. Biogenic synthesis of silver nanoparticles and their synergistic effect with antibiotics: A study against gram-positive and gram-negative bacteria. *Nanomed. Nanotechnol. Biol. Med.* **2010**, *6*, 103–109. [CrossRef]

36. Chopade, B.A.; Singh, R.; Wagh, P.; Wadhwani, S.; Gaidhani, S.; Kumbhar, A.; Bellare, J. Synthesis, optimization, and characterization of silver nanoparticles from Acinetobacter calcoaceticus and their enhanced antibacterial activity when combined with antibiotics. *Int. J. Nanomed.* **2013**, *8*, 4277–4290. [CrossRef]

37. Ruddaraju, L.K.; Pammi, S.; Guntuku, G.S.; Padavala, V.S.; Kolapalli, V.R.M. A review on anti-bacterials to combat resistance: From ancient era of plants and metals to present and future perspectives of green nano technological combinations. *Asian J. Pharm. Sci.* **2020**, *15*, 42–59. [CrossRef] [PubMed]

38. Pal, S.; Tak, Y.K.; Song, J.M. Does the Antibacterial Activity of Silver Nanoparticles Depend on the Shape of the Nanoparticle? A Study of the Gram-Negative Bacterium *Escherichia coli*. *Appl. Environ. Microbiol.* **2007**, *73*, 1712–1720. [CrossRef]

39. Martínez-Castañón, G.A.; Niño-Martínez, N.; Martínez-Gutierrez, F.; Martínez-Mendoza, J.R.; Ruiz, F. Synthesis and antibacterial activity of silver nanoparticles with different sizes. *J. Nanoparticle Res.* **2008**, *10*, 1343–1348. [CrossRef]

40. Zhang, M.; Zhang, K.; De Gusseme, B.; Verstraete, W.; Field, R. The antibacterial and anti-biofouling performance of biogenic silver nanoparticles by *Lactobacillus fermentum*. *Biofouling* **2014**, *30*, 347–357. [CrossRef] [PubMed]

41. Sondi, I.; Salopek-Sondi, B. Silver nanoparticles as antimicrobial agent: A case study on *E. coli* as a model for Gram-negative bacteria. *J. Colloid Interface Sci.* **2004**, *275*, 177–182. [CrossRef]

42. Dutta, R.; Nenavathu, B.P.; Gangishetty, M.K.; Reddy, A. Studies on antibacterial activity of ZnO nanoparticles by ROS induced lipid peroxidation. *Colloids Surf. B Biointerfaces* **2012**, *94*, 143–150. [CrossRef] [PubMed]

43. Meikle, T.G.; Dyett, B.P.; Strachan, J.B.; White, J.; Drummond, C.J.; Conn, C.E. Preparation, Characterization, and Antimicrobial Activity of Cubosome Encapsulated Metal Nanocrystals. *ACS Appl. Mater. Interfaces* **2020**, *12*, 6944–6954. [CrossRef] [PubMed]

44. Zhang, X.-F.; Liu, Z.-G.; Shen, W.; Gurunathan, S. Silver Nanoparticles: Synthesis, Characterization, Properties, Applications, and Therapeutic Approaches. *Int. J. Mol. Sci.* **2016**, *17*, 1534. [CrossRef] [PubMed]

45. Yin, I.X.; Zhang, J.; Zhao, I.S.; Mei, M.L.; Li, Q.; Chu, C.H. The Antibacterial Mechanism of Silver Nanoparticles and Its Application in Dentistry. *Int. J. Nanomed.* **2020**, *15*, 2555–2562. [CrossRef] [PubMed]